Phys Chem Minerals (2004) 31: 131–141
DOI 10.1007/s00269-003-0365-8

ORIGINAL PAPER

S. V. Churakov · B. Wunder

Ab-initio calculations of the proton location in topaz-OH, $Al_2SiO_4(OH)_2$

Received: 17 March 2003 / Accepted: 23 September 2003

Abstract The position of hydrogen in the structure of topaz-OH was determined by means of ab-initio quantum-mechanic calculations. Static lattice energy calculations predict the existence of four non-equivalent positions of protons, which are characterized by O4–H1…O1, O4–H2…O2, O4–H3…O3 and O4–H4…O4 hydrogen bonds. The distribution of the protons between positions of local equilibrium is controlled by the proton–proton avoidance rule and the strength of the hydrogen bonds. The most favourable configuration of hydrogen atoms is achieved for adjacent protons, which form O4–H3…O3 and O4–H4…O4 hydrogen bonds, respectively. The thermal excitation of atoms at a temperature of 55 K is large enough for the hydrogen atoms occasionally to change their positions to form O4–H1…O1 and O4–H2…O2 bonds. At ambient pressures and higher temperatures the protons are in a dynamic exchange between the allowed positions of local minima. As a consequence, for nearly room-temperature conditions, the dynamic change between different structural configurations leads to the violation of all possible symmetry elements and with that to space group *P*1. The flipping of the protons between different sites is achieved by simple rotation of the OH-dipole and does not produce any significant distortion of the framework of topaz, whose symmetry remains that of the space group *Pbnm*. Therefore, no reduction of symmetry has been observed in former X-ray studies on topaz-OH. Calculated IR absorption spectra of topaz-OH were found to be in good agreement with measured spectra. According to the calculations, the two favourable configurations of protons might correspond to the measured peak splitting within the OH-stretching range. An experimentally observed low-frequency band at 3520 cm^{-1} was assigned to the OH-stretching of the O4–H3…O3 bond, while the band at 3600 cm^{-1} was attributed to OH-stretching of the O4–H4…O4 hydrogen bond. The broad peak in FAR-IR frequency range at 100–150 cm^{-1} is attributed to the stretching of H3…O3 and H4…O4 contacts. The rate of proton exchange at 670 K among different sites was estimated by ab-inito molecular dynamic simulations. The calculations predict that flipping of adjacent protons between O4–H3…O3 and O4–H4…O4 bonds at 670 K occur at a rate of about 1.96 THz.

Keywords Topaz-OH · Ab-initio calculation · Proton location · IR spectroscopy

S. V. Churakov (✉)
Centro Svizzero di Calcolo Scientifico,
Via Cantonale, 6980 Manno,
Switzerland; Department of Chemistry,
ETH, Hönggerberg HCI,
8093 Zurich, Switzerland
e-mail: churakov@cscs.ch
Tel.: +41 91 610 8222
Fax: +41 91 610 8282

B. Wunder
GeoForschungsZentrum Potsdam,
Division 4, Telegrafenberg,
14473 Potsdam, Germany

Introduction

Fluorine-dominated topaz, $Al_2SiO_4(F,OH)_2$, occurs as an accessory mineral in aluminous- and fluorine-rich rocks, which, in principle, are formed at low pressures. Topaz of an X_{OH} content of up to 0.55, which is the highest ever found in nature, has recently been described for an occurrence in ultrahigh-pressure rocks of the Sulu terrane, Eastern China (Zhang et al. 2002). The OH endmember of topaz (topaz-OH), $Al_2SiO_4(OH)_2$, was first synthesized by Wunder et al. (1993) in multi-anvil experiments at high pressures above 7.0 GPa. This phase, up to now not found in nature, is proposed to be an important water-containing mineral in deeply subducted pelitic sediments and basaltic materials (Schreyer 1995; Schmidt 1995; Domanik and Holloway 1996). Additionally, it has been proposed that the variation of the F,OH contents in topaz with pressure and temperature might be used as a geothermobarometer (Barton

1982; Wunder et al. 1999; Ferrando et al. 2002). However, the F,OH solid solution series in topaz can be described reliably only by a thermodynamic model, when structural uncertainties of topaz-OH and of intermediate F,OH members of topaz are solved. For a description of the F,OH solid solution of topaz, Barton (1982) derived the "proton-avoidance" activity-composition model. This model followed structural considerations by Gebert and Zemann (1965) that, due to H–H repulsion, the maximum X_{OH} of topaz should be 0.5. Due to the findings of OH-rich topaz with $X_{OH} > 0.5$ in high-pressure rocks and the synthesis of topaz with $X_{OH} > 0.5$ and of topaz-OH, this old concept has to be reconsidered.

Wunder et al. (1993) investigated the structure of topaz-OH by single-crystal X-ray diffraction, but were not able to locate the position of hydrogen from the Fourier difference synthesis. According to Northrup et al. (1994), as the result of proton repulsion, two non-equivalent OH positions should exist in the structure of topaz-OH. This would lead to a reduction of symmetry of space group (SG) *Pbnm*, known for natural, normally F-rich topaz, to SG $Pbn2_1$, by loss of the mirror plane in (001). IR characterization of topaz-OH (Wunder et al. 1993) in the OH-stretching vibration region indicated two sharp maxima at 3602 and 3526 cm^{-1} and a broad band at about 3457 cm^{-1} (see Fig. 4c). IR spectra of synthetic topaz of $X_{OH} > 0.5$ revealed the existence of topaz-OH components (Wunder et al. 1999). These observations point to more than one structurally non-equivalent OH position in OH-dominated topaz and indicate the proposed reduction in symmetry compared to natural OH-poor topaz and synthetic topaz of $X_{OH} < 0.5$ (Wunder et al. 1999), for which only one sharp OH band can be observed in the IR spectra.

The aim of this study was to determine the positions of protons for the topaz-OH structure by ab-initio quantum-mechanic structure optimization calculations. We also predicted the IR spectrum of topaz-OH/OD and the proton density distribution of the topaz structure at different temperatures. Additionally, the rate of proton exchange between different crystallographic sites was estimated from molecular dynamic calculations.

Methods

Static lattice energy calculations

Static 0-K structure optimizations have been carried out using the CPMD-3.5 density functional (DFT) code (CPMD 1990–2001). The calculations were accomplished with the BLYP exchange-correlation functional (Becke 1988; Lee et al. 1988) utilizing the generalized gradient approximation (GGA). Non-local norm-conserving Goedecker-type pseudopotentials (Goedecker et al. 1996) were applied to account for core electrons. Valence electron orbitals were approximated by plane wave expansion with a 1630-eV plane wave energy cutoff. The valence electron states for Al, Si, O and H were $3s^23p^1$, $3s^23p^2$, $2s^22p^4$ and $1s^1$, respectively. A $2 \times 1 \times 1$ supercell containing 88 atoms [8 $Al_2SiO_4(OH)_2$] was used in the calculations.

The relaxation of the atomic positions was performed for the fixed geometry of the orthorhombic unit cell ($a = 4.719$ Å; $b = 8.918$ Å; $c = 8.416$ Å, $Z = 4$) of topaz. The structure parameters of topaz determined by Northrup et al. (1994) were used as the initial structure model of the calculations. The lattice energy determination was performed in several steps continuously increasing the accuracy of the calculations. As a first step, the optimal positions of hydrogen atoms in the topaz structure were searched using a cell of 44 atoms by applying a Γ-point energy sampling and 950-eV cutoff. As the next step, the geometry of the obtained configuration was refined using the $2 \times 1 \times 1$ supercell with a 1630-eV cutoff. Finally, the lattice energies of the predicted structure in $2 \times 1 \times 1$ supercell were calculated on a $16 \times 16 \times 16$ Monkhost–Pack mesh (Monkhorst and Pack 1975) using the density functional perturbation theory after Iannuzzi and Parrinello (2001).

Any ab-initio simulation exposes a few approximations, which have to be treated carefully to obtain accurate results. The parameters to control are a model for the exchange-correlation functional, pseudopotentials, number of plane waves and the k-point in the Brilloin zone used for the energy calculations. We utilized the gradient-corrected exchange-correlation functional (GGA), which is known to give the best performance for systems with weak hydrogen bonding (Sprik et al. 1996). However, GGA is also known to overestimate the lattice parameters of solids by a few percent (e.g. Karki et al. 1997) systematically. This effect can be minimized by fixing the lattice parameters at the experimentally determined values. To estimate the accuracy of the energy calculations in this study, we express the exact energy difference E_{tot} between the structures A and B as follows:

$$\Delta E_{tot} = [E^A_{960eV} - E^B_{960eV}] + [\Delta E^A_{1630eV} - \Delta E^B_{1630eV}] + [\Delta E^A_p - \Delta E^B_p] + \Delta E_{err} \quad (1)$$

E_{960eV} is the lattice energy obtained from the Γ-point calculations with a 960-eV plane wave cutoff. ΔE_{1630eV} is the energy due to the cutoff increment from 960 to 1630-eV. ΔE_P is the perturbation energy due to k-point sampling. The deviation from the actual energy difference ΔE_{err} is given by errors in the plane wave expansion and the k-point sampling. The uncertainty of the plane wave expansion is smaller than $[\Delta E^A_{1630eV} - \Delta E^B_{1630eV}]$ and the k-point sampling is 1 order of magnitude more accurate than $[\Delta E^A_p - \Delta E^B_p]$. In Table 1 the corresponding energies are given. The maximal $[\Delta E^A_{1630eV} - \Delta E^B_{1630eV}]$ difference is below 1 kJ mol^{-1}. The maximal $[\Delta E^A_p - \Delta E^B_p]$ difference is 0.6 kJ mol^{-1}. The total accuracy of the energy calculation with respect to the plane wave expansion and k-point sampling is better than ± 1.1 kJ mol^{-1}. To check the accuracy of the geometry optimization, we compared the bond length of the structures optimized with 960- and 1630-eV plane wave cutoff. The differences were below 0.01 Å for Si–O, Al–O and O–H bonds and 0.02 Å for O…H distances. As the k-point sampling correction to the energy is 1 order of magnitude smaller than the one for the plane wave basis set, the effect of k-point sampling on the geometry optimization can be neglected. Finally, we performed lattice energy calculations on one of the optimized structures using Troullier and Martins (1991) norm-conserving pseudopotentials. These resulted in no significant difference in the structure geometry.

Molecular dynamic simulations

In order to study dynamic properties of hydrogen in topaz-OH, a series of microcanonical Car–Parrinello molecular dynamic simulations (Car and Parrinello 1985) were performed at average temperatures of 55, 270 and 665 K. To allow longer integration steps, the hydrogen atoms were substituted with deuterium. The simulations were done with a $2 \times 1 \times 1$ supercell, using Γ-point sampling. The valence wave function was expanded in plane wave up to 960-eV energy cutoff. The core electrons were approximated with Troullier and Martins (1991) norm-conserving pseudopotentials. Equations of motion were integrated with 0.12-fs time steps. The

Table 1 Energies, symmetries and bond lengths (Å) of topaz-OH structures calculated with $2 \times 1 \times 1$ supercell. Absolute energy of the structure T4 is set to zero. ΔE *(*Γ*, 950 eV)* Lattice energy after Γ-point geometry optimization with 950-eV plane wave cutoff; ΔE(Γ, *1630 eV)* improved calculations with 1630-eV plane wave cutoff; ΔE_p*(1630 eV)* energy contribution due to k-point sampling. $\mathbf{\Delta E_{tot}(1630\ eV)} = \Delta E$(Γ, *1630 eV)* + ΔE_p*(1630 eV)* total energy difference relative to the structure T4

Structure	T4	T3	T1	T2[a]	T5
Symmetry	$P2_1/b$	$Pbn2_1$	*Pbnm*	*Pbnm*	$P2_1/b$; $Pbn2_1^b$
ΔE(Γ, 950 eV) (kJ mol^{-1})	0.00	−0.15	4.00		
ΔE(Γ, 1630 eV) (kJ mol^{-1})	0.00	0.58	3.1		−2.49
ΔE_p(1630 eV) (kJ mol^{-1})	0.00	−0.30	0.2		−0.57
ΔE_{tot}(1630 eV) (kJ mol^{-1}]	**0.00**	**0.28**	**3.3**		**−3.06**
< Si–O1 >	1.65	1.64	1.64	1.66	1.65
< Si–O2 >	1.66	1.66	1.66	1.67	1.66
< Si–O3 >	1.64	1.65	1.65	1.65	1.64
< Si–O4 >					
< Al–O1 >	1.97	1.96	1.93	1.99	1.97
< Al–O2 >	1.95	1.95	1.97	1.93	1.95
< Al–O3 >	1.92	1.92	1.92	1.93	1.92
< Al–O4 >	1.84	1.84	1.84	1.83	1.84
< O4–H1 >	0.97	0.97		0.99	
< O4–H2 >	0.97	0.97	0.97		
< O4–H3 > / < O4–H4 >					0.98/0.97
< H1..O1 >	2.03	2.16		1.97	
< H1..O2 >	2.28	2.34		2.25	
< H1..O3 >	2.24	2.25		2.22	
< H1..O4 >	2.36	2.30		2.43	
< H2..O1 >	2.35	2.34	2.30		
< H2..O2 >	2.02	2.07	2.04		
< H2..O3 >	2.30	2.27	2.32		
< H2..O4 >	2.47	2.39	2.40		
< H3..O1 > / < H4..O1 >					2.32 / 2.44
< H3..O2 > / < H4..O2 >					2.45 / 2.30
< H3..O3 > / < H4..O3 >					1.80 / 2.40
< H3..O4 > / < H4..O4 >					2.20 / 2.20
< H … H >	2.06	2.04	1.89	1.67	2.28

[a] The structure T2 was obtained in calculation with a single unit cell of topaz only, and could not be reproduced using a $2 \times 1 \times 1$ supercell (see text for details)

[b] Actual lattice structure is *P*1, but different structure motifs can be identified (see text for details)

fictitious electron mass was assigned to 900 a.u. The production runs of about 15 ps were followed by 1 ps equilibration starting from the equilibrium configuration T3 (see later). One microcanonic MD run was performed on topaz-OH without isotopic substitution at an average temperature of 298 K. The fictitious electron mass was assigned to 600 a.u. and the equation of motion was integrated with a time step of 0.1 fs. The nuclei were treated classically through the simulation. This is a crude approximation for light atoms like D and H at low temperature. Taking quantum effects into proper account in our simulation might allow for tunnelling of deuterium atoms between the position of local energy minima at 55 K. However, the latter does not affect the basic conclusions of the paper.

IR spectra

We calculated the infrared absorption spectrum, $a(\omega)n(\omega)$, of topaz-OH from the Fourier transform of the time correlation function, $\langle \mathbf{M}(t) \cdot \mathbf{M}(0) \rangle$, of the total (ionic and electronic) dipole moment of the system according to Silvestrelli et al. (1997) by Eq. (2):

$$a(\omega)n(\omega) = \frac{4\pi\omega \tanh(\beta\hbar\omega/2)}{3\hbar c V} \times \int_{-\infty}^{\infty} \langle \mathbf{M}(t) \cdot \mathbf{M}(0) \rangle e^{-i\omega t} dt \ , \quad (2)$$

where $a(\omega)$ is the absorption coefficient, $n(\omega)$ the refractive index, V the volume, $\beta = (k_B T)^{-1}$, T the temperature, k_B the Boltzmann constant and c the speed of light. The electronic contribution is calculated in the CPMD program using the Berry phase scheme (Silvestrelli et al. 1997) and the spectrum was obtained using the maximum entropy method (e.g., Press et al. 1992). For characterization of the IR bands, we performed a finite difference vibration analysis using the single unit cell of topaz and the calculated phonon density of state for every single atom based on the velocity autocorrelation function obtained from the dynamic trajectories.

The validity of the semiclassical quantum correction factor $\tanh(\beta\hbar\omega/2)$ in Eq. 2 has been discussed in detail by Silvestrelli et al. (1997). They showed that Eq. 2 underestimates by up to 60% the absorption intensity in the far-IR part of the spectra. However, a more sophisticated treatment of the quantum correction like the Egelstaff procedure (Egelstaff 1962) is not valid for the middle-IR range (Borysow et al. 1985). Since we are primarily concerned with the relative positions of the absorption peaks rather than the intensities, we therefore assume that more accurate quantum corrections are not necessary.

For a fair comparison of the calculated IR absorption spectra of topaz-OD with the experimental data of topaz-OH, the frequency scale of the calculated spectra must be corrected for the isotope effect and inertia for the fictitious electron dynamics on the high-frequency vibrations (Blöchl and Parrinello 1992). In a harmonic approximation, the frequency shift due to the substitution of hydrogen by deuterium can be expressed as:

$$\nu_H = \sqrt{\frac{M_D}{M_H}} \nu_D \approx 1.4 \nu_D \ , \quad (3)$$

where ν_H, M_H and ν_D, M_D are frequencies and masses of hydrogen and deuterium, respectively. Applied to our system, the correction

is an approximation since normal modes do not involve hydrogen atoms only. For correction of the fictitious electron dynamics, we performed a series of microcanonical ab-initio MD simulations of an isolated D_2 molecule at low temperatures to maintain harmonic vibrations. The vibration frequencies calculated from velocity autocorrelation decreased at higher fictitious electron masses. At 900 a.u. the calculated frequency was 2905 cm^{-1}, against the experimental value of 3115.5 cm^{-1} (Terhune and Peters 1959). This indicates that the calculated frequency spectra of topaz-OD must be scaled by a factor of 1.07. Similar simulations have been performed for H_2 molecules with a fictitious electronic mass of 600 a.u. The obtained vibration frequency was 4025 cm^{-1} against the experimentally measured value of 4401 cm^{-1} (Terhune and Peters 1959) resulting in a scale factor of 1.093.

The radial distribution function (RDF) and the three dimensional distribution of the proton density was calculated based on atomic trajectories produced in the MD simulation runs. To remove the cell drift during MD simulations, movement of the centre of mass of the simulation box was subtracted from atomic trajectories.

Results and discussion

Ab-initio structure optimization

The projections of optimized structures of topaz-OH corresponding to the local minima of the lattice energy obtained at 0 K are shown in Fig. 1. The relative lattice energies, symmetry and bonds length are summarized in Table 1.

The second smallest static lattice energy was obtained for the structure T4, where the hydrogen atoms were found to occupy two different positions, H2 and H1, with (x, y, z) coordinates (0.06, 0.22, 0.15) and (0.88, 0.33, 0.34), respectively. Ordering of these hydrogen atoms in the lattice would violate the mirror plane m and glide plane n of the SG *Pbnm* and the symmetry would be lowered to the monoclinic space group $P2_1/b$. Atoms in the H2 positions are involved in O4–H2…O2 hydrogen bonds while H1 sites form O4–H1…O1 bonds.

The calculated energy of the structure T3 is only 0.28 kJ mol^{-1} higher than the energy of the T4 structure. This difference is within the accuracy of the energy calculations. Therefore, the T3 geometry can be considered as energetically equivalent to structure T4. The protons occupy practically the same crystallographic positions H2 and H1 with (x,y,z) coordinates (0.06, 0.21, 0.14) and (0.90, 0.31, 0.33). However, the ordering of hydrogen atoms is different and corresponds to the higher symmetry of SG $Pbn2_1$. This SG has been assumed by Northrup et al. (1994) for topaz-OH. Similarly to the T4 structure, the H2 sites form O4–H2…O2 bonds and H1 builds O4–H1…O1 contacts.

The structure T1 is 3.3 kJ mol^{-1} higher in energy than configuration T4. All eight hydrogen atoms are situated in the H2 site with coordinates (0.05, 0.22, 0.14), while the H1 site remains unoccupied. This ordering of hydrogen atoms leads to SG *Pbnm*. The protons form short O4–H2…O2…H2–O4 and long O4–H2…O1…H2–O4 bonds. In contrast to the configurations T3 and T4, the distance between two protons is rather short (see Table 1), which might explain the higher lattice energy.

Structure T2 was obtained in a preliminary geometry optimization using the single unit cell of topaz (44 atoms) and the 950-eV plane wave cutoff. Further attempts to reproduce the T2 geometry with $2 \times 1 \times 1$ supercell have failed. Starting in a framework of a $2 \times 1 \times 1$ supercell with the T2 configuration, the geometry optimizations ended up with either T3 or T4 geometries. Therefore, there is no accurate energy calculation available for the T2 configuration. Notwithstanding these technical complications, we assume the geometry of the T2 structure as an important hypothetical structure of topaz-OH where all hydrogen atoms are ordered in the H1 positions. The bond geometry reported for T2 may not be very accurate and must be considered with care. The symmetry of the T2 structure can be assigned to SG *Pbnm*. Hydrogen atoms form strong O4–H1…O1…H1–O4 bonds and weaker O4–H1…O3 contacts. One particular feature of the structure T2 is its very short H…H distance of about 1.67 Å. This might explain the observed instability of this configuration. Obviously, such a short distance between protons is unfavourable, and a small perturbation of atomic positions displaces the system from local equilibrium to lower energy states.

Structure T5 was found to have the lowest lattice energy among all obtained structures. This geometry was obtained using a simulated annealing optimization technique and therefore reflects the global energetic minima of the topaz-OH structure to a high confidence. The hydrogen atoms were localized in two positions (0.07, 0.17, 0.07) and (0.99, 0.27, 0.32) referred to as H3 and H4, respectively. Ordering of hydrogen atoms violates every symmetry element of primary *Pbnm* symmetry and the SG of this structure must be assigned to $P1$. A closer look at the geometry shows that long-range proton ordering implies superposition of the structural motifs observed in the T3 and T4 geometries maintaining SG $Pbn2_1$ and $P2_1/b$, respectively. This long-range proton ordering will be discussed in more detail in the coming section based on the results of the MD runs. A particular feature of this configuration is the extremely short O4–H3…O3 bond. Orientation of the O4–H4 bond is ruled by O4–H4…O4 and somewhat longer O4–H4…O2 hydrogen bonds. The low energy of this structure can be explained by the long H…H distance (2.28 Å), which is significantly increased compared to the H…H distance of all other calculated structures.

To summarize, the results of the static geometry optimization predict that the orientation of every OH dipole is determined by four different hydrogen bonds O4–H1…O1, O4–H2…O2, O4–H3…O3 and O4–H4…O4. The local distribution of the adjacent protons is controlled by the proton–proton avoidance rule. The maximal separation of protons is achieved when hydrogen is distributed between H3 and H4 sites. On the instance of the structures T3 and T4, we see

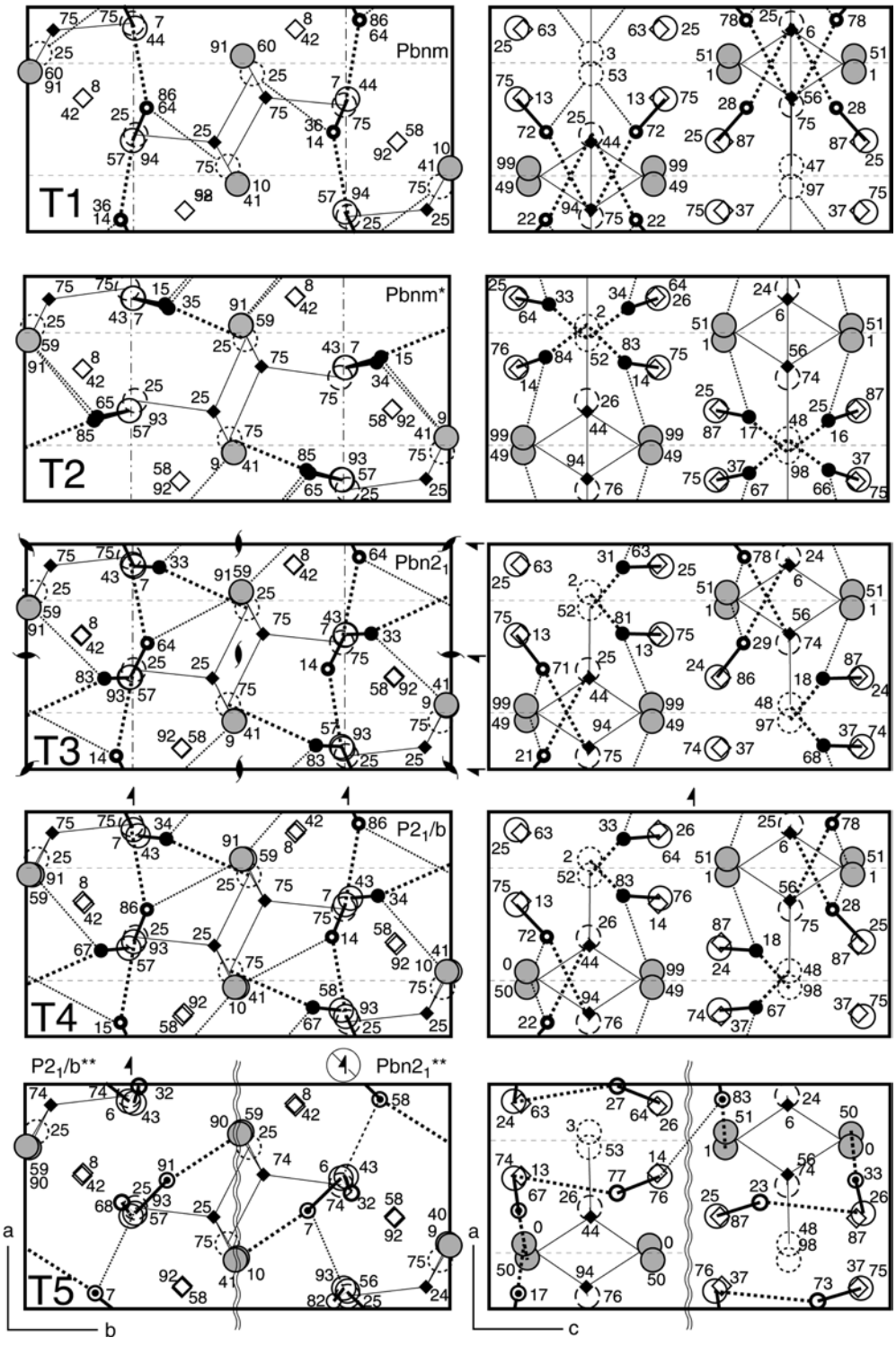

Fig. 1 *ab*, *ac* and *bc* projection of optimized structures of topaz-OH. The *dotted lines* represent the two shortest H…O bonds. The *bolder dotted lines* indicate shorter bonds (see Table 1 for details). The *numbers near the symbols* indicate height of atoms in direction perpendicular to the projection plane. Units are fractional height × 100. * Projections of the configuration T2 show small distortions violating symmetry elements of SG *Pbnm*. These deviations are attributed to the low accuracy of the calculations in that particular case (see text for details). ** The long-range disorder of protons in T5 corresponds to the SG *P*1. A closer look on the structures turn out that protons are partly ordered according to $Pbn2_1$ and $P2_1/b$ (see Discussion for details)

that long-range ordering does not have any significant effect on the static lattice energy. Therefore, for a given distribution of adjacent protons between non-equivalent sites, the structure of topaz-OH may have SG *P*1 as in T5, $Pbn2_1$, as in T3 or $P2_1/b$ as in T4. At finite temperatures, long-range disorder of proton pairs will be favourable because of the entropy effect.

Proton dynamics at finite temperatures

Calculated O–D(H) radial distribution functions (RDFs) of topaz at different temperatures are shown in the Fig. 2. There is a very good agreement between RDF calculated for topaz-OD and topaz-OH at 270 and 298 K, respectively. Therefore, in the following we

Fig. 1 (Contd.)

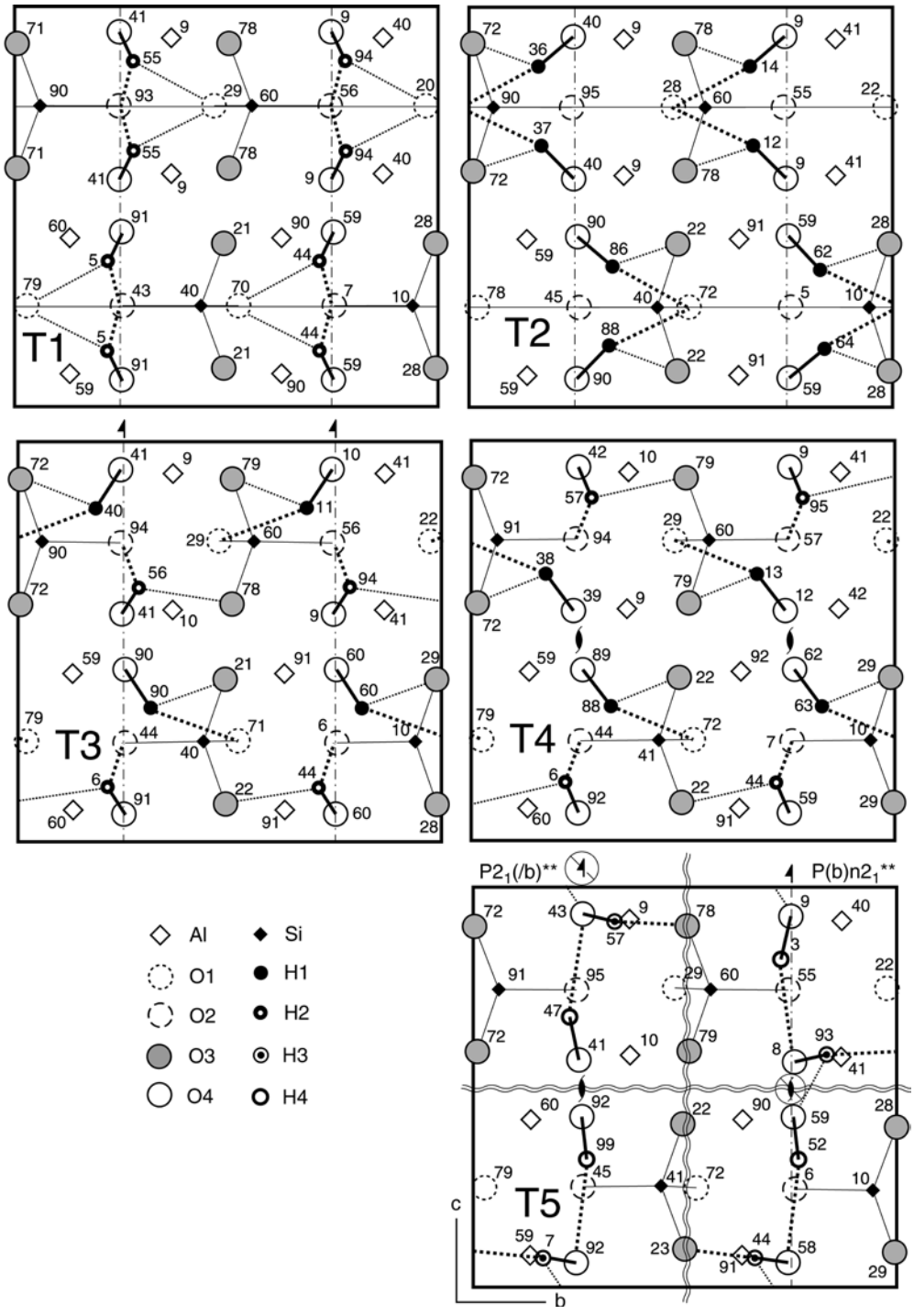

do not distinguish between hydrogen and deuterium. However, it has to be remembered that at low temperature (55 K) quantum effects enhance the mobility of H/D, resulting in broadening of RDF peaks. Remarkable differences between O–H RDFs obtained at 55 K and higher temperatures are observed. The 55-K RDF peaks are rather sharp while for the high-temperature distributions the peaks are more diffuse. The peaks of the RDFs can be identified using the results listed in Table 1. The peak at 1.8 Å for the O3–H RDF is associated with H3 sites. The hydrogen atoms located in H2 and H1 sites produce peaks at about 2.05 Å on O2–H and O1–H RDFs, respectively. The H4 site is more difficult to identify because the characteristic peaks overlap with the peaks originated from other sites.

At 55 K there is almost no sign of the protons located in the sites H2 and H1. The sharp peak at 1.8 Å

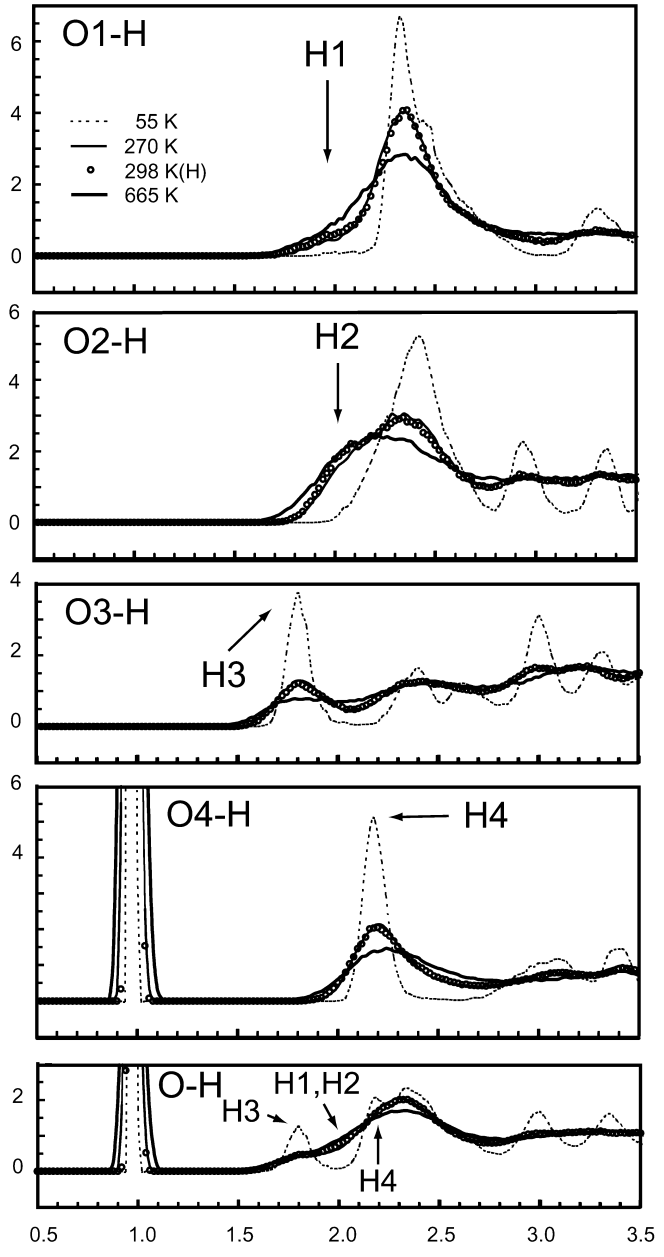

Fig. 2 O(*n*)- D and O(*n*)-H radial distribution functions of topaz-OH(D) at different temperatures

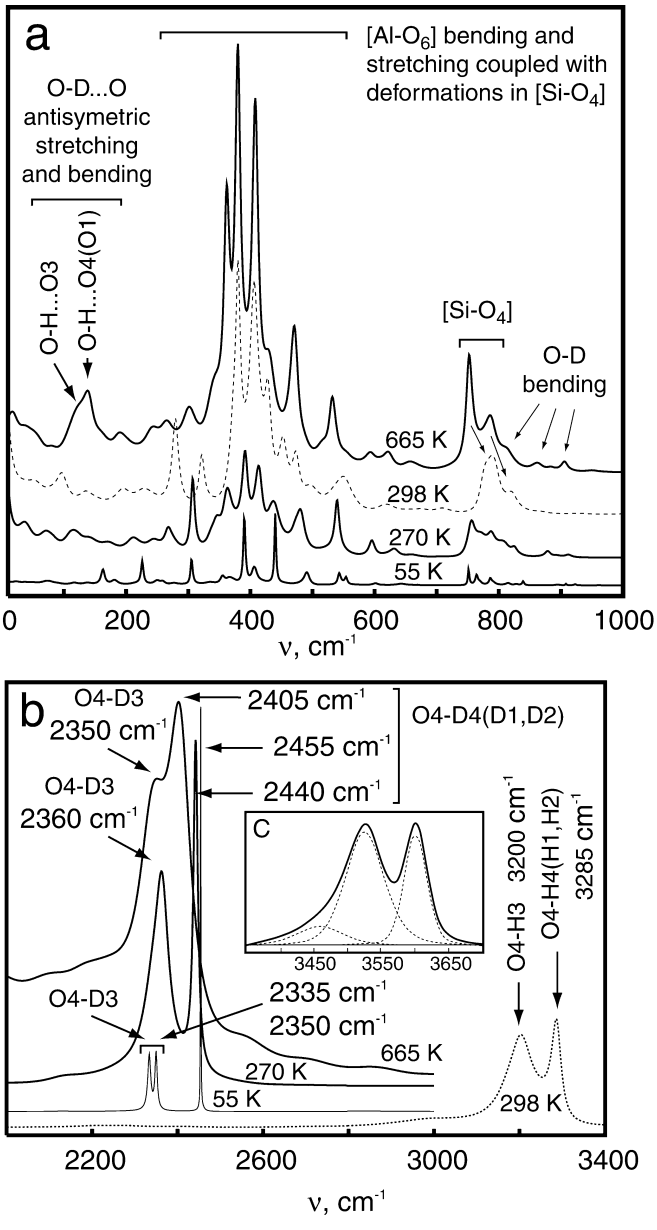

Fig. 3 Calculated IR spectra of topaz-OD (**a**, **b**) at 55, 270 and 665 K (*solid lines*). The corresponding IR spectra of topaz-OH (**a**, **b**) at 298 K are shown by *dashed lines*. The measured IR adsorption spectra of topaz-OH after Wunder et al. (1993) is shown in **c**

on the O3–H RDF indicates a high concentration of protons in the H3 site. Because of H–H repulsion, the neighbouring hydrogen atom cannot simultaneously occupy H3 sites. Therefore at 55 K, only one half of hydrogen atoms are located in the H3 sites; the others occupy the H4 positions. At 270 and 665 K the first peak on the O1–H RDFs has a long shoulder at about 2.05 Å produced by the protons in the H1 site. Similarly, there are broad peaks near 2.05 Å on O2–H RDFs originated from the H2 site. These observations indicate that at higher temperatures the protons are disordered among H1, H2, H3 and H4 sites and can, in principle, change their location with time.

Calculated IR spectra

Calculated infrared spectra of topaz-OD and topaz-OH at different temperatures are shown in the Fig. 3. The differences in the position of O–D and O–H stretching and bending modes might be explained by the isotope effect. The slight shift to higher frequencies of other vibration bands of topaz-OH relative to that of topaz-OD might be due to the smaller fictitious electronic mass of topaz-OH relative to topaz-OD.

Two peaks in the range 750–800 cm^{-1} are attributed to stretching vibrations of the [SiO_4] tetrahedra. In topaz-OD these bands overlap with the O–D bending

modes. The series of sharp bands in the range 300–600 cm^{-1} are produced by the stretching and bending of [AlO_6] octahedra coupled with the bending modes of [SiO_4] tetrahedra. This part of the spectra is very complex and does not allow a simple interpretation without detailed normal mode analyses, which, however, was not with in the scope of our study.

Two peaks near 2300 cm^{-1} for topaz-OD and near 3200 cm^{-1} for topaz-OH can be undoubtedly associated with O–D and O–H stretching, respectively. Spectra at 270 and 600 K show two well-defined peaks with a shape similar to the measured spectra of topaz-OH as shown by Wunder et al. (1993). Scaling the calculated frequencies of topaz-OD by a factor 1.4×1.07 and by the factor 1.093 for topaz-OH (see section Methods: IR spectra), we obtained two peaks at 3520 and 3603 cm^{-1} for the 665-K spectra; peaks at 3535 and 3655 cm^{-1} for 270-K spectra and peaks 3498 and 3591 cm^{-1} for 298 K. These values are in good agreement with the positions of the split OH-stretching vibrations near 3520 and 3600 cm^{-1} reported by Wunder et al. (1993) for topaz-OH. The power spectra of the one-atom autocorrelation function indicate that the peak at lower frequency is the O4–H3 vibration. The peak at high frequencies is produced by the H1, H2 and H4 sites.

The spectrum obtained at 55 K shows a splitting of the low-frequency peak to two bands at 2335 and 2350 cm^{-1}. In order to identify the nature of these peaks, we calculated separate H-O*n* RDF for each of the 16 hydrogen atoms in the supercell. These calculations indicate that the atoms are arranged in four by four groups producing similar RDF and phonon density of state. Average RDFs for each of these groups are shown in Fig. 4. A sharp peak at 1.8 Å for the O3–D RDF indicates that the distributions A and B result from atoms at H3 positions. The intensity of the peak for distribution B is almost 30% lower, however. Moreover, distribution B gives a small peak at 2.05 Å on the O2–D, which can be attributed to the H2 site. Deuterium atoms producing distribution A might be attributed to a pure H3 state. These atoms are responsible for the band at 2335 cm^{-1}. The distribution B is given by disturbed O4–H3…O3 bonds and will produce somewhat higher frequencies at 2350 cm^{-1}. Indeed, the H3 position is characterized by an O4–H3…O3 bond with an extremely short H3…O3 contact of 1.8 Å. The shorter the O…H contact the weaker the H–O bond, and as a consequence the lower the O–H-stretching frequencies. The distributions C and D result from atoms at H4 sites. These distributions also have the signature of H1 and H2 sites as observed in the O1–H and O2–H RDF. The vibration frequencies associated with these sites are similar, which indicates that the force constants of the O…H contacts are approximately the same.

At 665 K two broad IR bands can be observed, which formed by superposition of the peaks near 120 and 140 cm^{-1}. The power spectra of the single atom velocity autocorrelation function indicate that these peaks in the FAR-IR region result from hydrogen

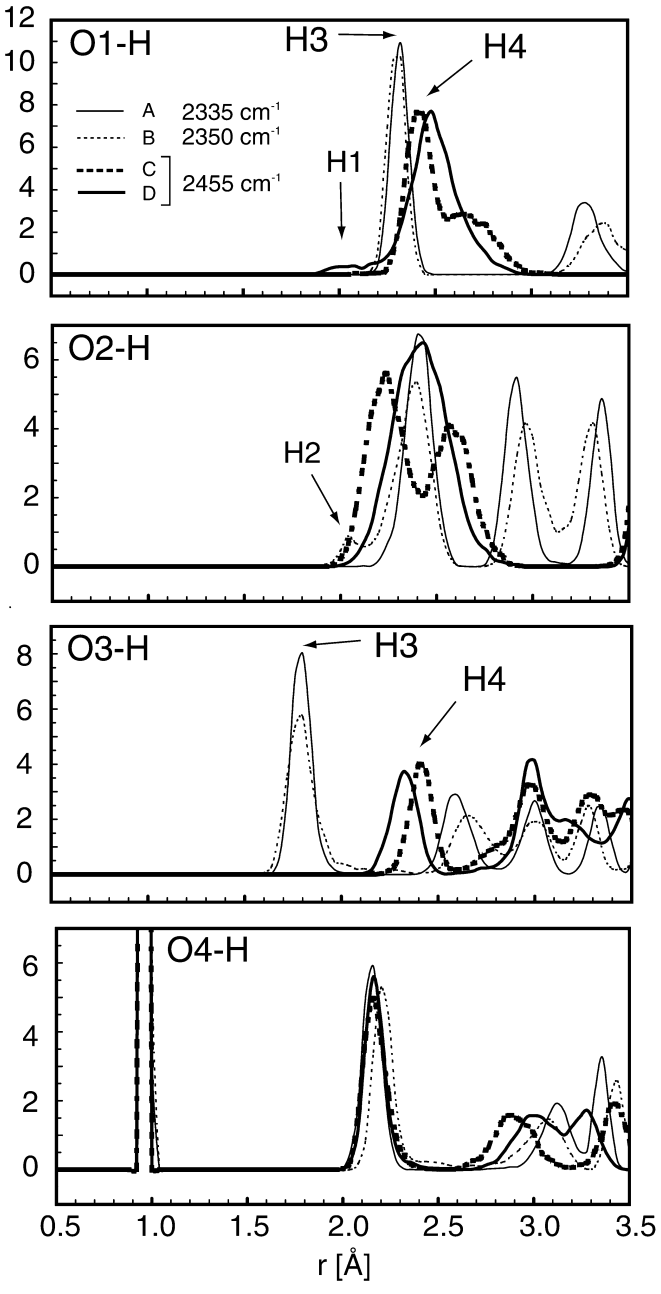

Fig. 4 Detailed O(*n*)-D radial distribution function of topaz-OD at 55 K. The 16 separate distributions were calculated for every deuterium atom in the supercell. Average was taken among atoms (four atoms for every line) showing similar distribution functions and which are responsible for the same phonon frequencies in the vibrational density of states

motion. In liquid deuterium water a broad adsorption peak near 165 cm^{-1} was reported by Silvestrelli et al. (1997) to be attributed to antisymmetric hydrogen bonding stretching. This might indicate that the observed vibrations in topaz are due to stretching of hydrogen bonds O–H…On. To check this hypothesis, we introduced a dipole moment $M_s = eR$. R is the vector pointing from H to the O*n* (n = 1,2,3,4) of the hydrogen bond O–H…On and e is electric charge associated with the dipole. The power spectra of the autocorrelation

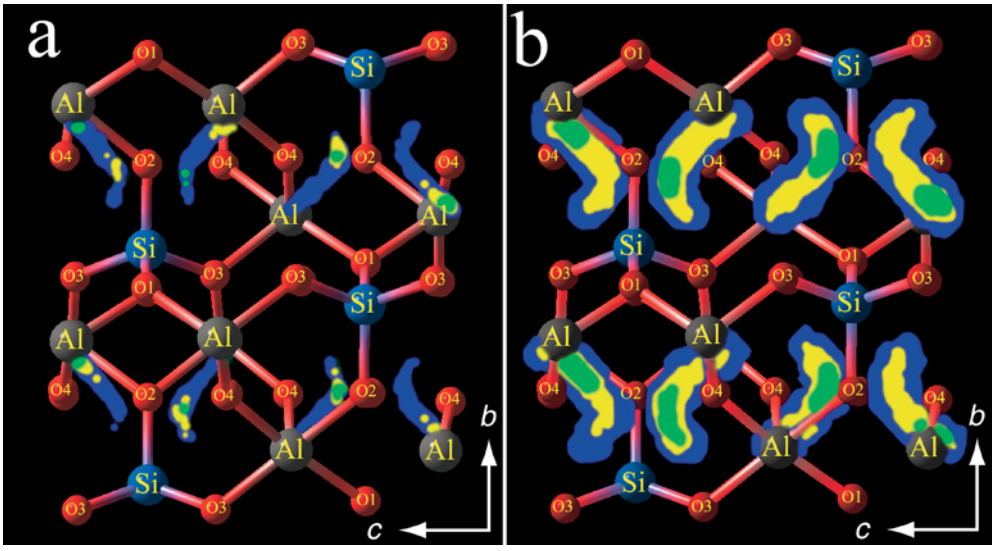

Fig. 5a, b YZ projection of the 3-D proton, density distribution in the unit cell of topaz-OD determined at 55, 270 and 665 K. The density distribution is superposed with a snapshot of a dynamic trajectory of topaz-OD at 55 K. *Green*, *yellow* and *violet areas* show the region of proton residence with 75% probability (**a**), and the entire region visited by deuterium atoms (**b**) at the temperatures 55, 270 and 665 K, respectively

functions $C_s(t) = [\mathbf{M}_s(t) \cdot \mathbf{M}_s(0)]$ calculated for O–D…O3 bonds show a strong peak at 120 cm^{-1}. The corresponding power spectra of O–D…O2 and O–D…O4 match the band at 140 cm^{-1}.

3-D proton density distribution calculations

From the oxygen–hydrogen RDF we noticed that the hydrogen atoms are mainly localized in the sites H3 and H4. For increasing temperatures, the atoms become more and more mobile, visiting H2 and H1 sites as well. In order to analyze the proton mobilities in more detail, we calculated three-dimensional proton density distributions. In Fig. 5a the surfaces of comprising regions with 75% probability of proton location are shown for the 55, 270 and 665 K MD runs. The proton distribution at 55 K confirms that the hydrogen atoms remain trapped in the H3 and H4 states. At 270 K several attempts were made by the atoms to leave the ground state and visit the H2 and H1 sites. The 665-K distribution is symmetric for adjusted atoms. This suggests that the neighbouring protons are free to move between H1, H2, H3 and H4 sites. In Fig. 5b the 3-D space visited by protons is shown for 55, 270 and 665 K MD runs. Even at the low temperature of 270 K the distribution for adjacent atoms is symmetric and therefore proton flipping between H1, H2, H3 and H4 sites takes place.

The proton density distributions at 55 and 270 K indicate that one of the adjacent protons is preferentially located in the H3 site while another is resident in H4 and with a lower probability in H1 and H2 positions. The static lattice energy calculations predict that simultaneous occupation of equivalent sites for neighbouring protons (both in H2 as in the T1 structure or both in H1 as in the T2 structure) is energetically unfavourable. It can be seen from the projections given in Fig. 1 that adjacent O–H dipoles located in non-equivalent sites form substantially different angles with the crystallographic *b* axis of topaz. Thus, the projection of the O–H vector on the *b* axis can be taken as a parameter characterizing whether an atom occupies H3(H1) or H4 (H2) sites. An example of the time evolution of the parameters $f_i(t) = \cos(\angle \vec{b}\vec{\mathrm{OH}}_i)$ for a pair of OD dipoles at 665 K is shown in the Fig. 6. The sign change of each function indicates the transition of the hydrogen atoms from site H3 to H4 or backward. The $f_i(t)$ for adjacent protons are anticorrelated in time, indicating that neighbouring atoms avoid occupation of equivalent sites.

To estimate the rate of proton exchange between different crystallographic sites we define $h(t)$ — a reaction coordinate of the proton transfer between sites H3(H1) and H4 (H2) — as follows:

$$h(t) = \begin{cases} 1, & \text{f1 (t)} \geq \text{f2 (t)} \\ -1, & \text{f1 (t)} < \text{f2 (t)}' \end{cases} \quad (4)$$

where the subscripts 1 and 2 refer to the adjacent atoms. The time evolution of $h(t)$ is also shown in the Fig. 6.

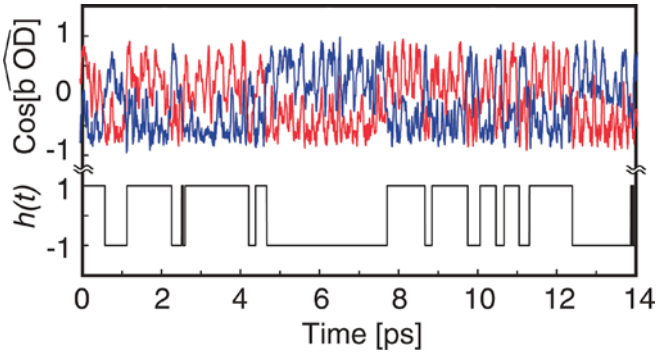

Fig. 6 *Red* and *blue lines* show evolution of angles formed by two adjacent OD dipoles with *b* axis as function of time. The sign change of the reaction coordinate $h(t)$, defined by the Eq. (4) traces the flipping event of adjacent deuterium atoms between positions H3 (H1) and H4 (H2)

The meaning of $h(t)$ is straightforward. Should $h(t)$ change its sign, one hydrogen atom has escaped the site H3 and the neighbouring proton has occupied the H3 site. The average rate of the transition k_D in topaz-OD at 665 K was found to be 1.4 THz. This transition can be thought as a bending near 24 cm^{-1} = $0.5k_D$ (to calculate the period of vibration, a sum of the time needed for the H3 ⇒ H4 transition and reverse H4 ⇒ H3 flipping is to be taken). Indeed one can see a broad band in the high-temperature far-IR that can be attributed to this motion.

In the transition state theory the reaction rate is calculated as: $k = v \cdot \exp(-\beta E_a)$, where E_a is the activation energy of the transition, $\beta = k_B T$ with k_B is the Boltzmann constant, T the temperature and v is the prefactor, which is thought of as the frequency at the transition state. The only parameter depending on the atomic masses is v. As a first approximation v can be treated as a normal vibrational motion and the isotope effect is calculated as the square root of the fraction of the atomic masses. Thus we estimate the transition rate for topaz-OH at 665 K to be $k_H \sim 1.4k_D$ = 1.96 THz.

Symmetry of topaz-OH

MD simulation is a unique tool, allowing real-time monitoring of atomic motion. The results of our calculations indicate that there are four non-equivalent crystallographic sites for protons in the structure of topaz-OH. At ambient conditions and high temperatures the protons are in a dynamic exchange between the crystallographic sites observed in configurations T3, T4 and T5. Instantaneous distribution of adjacent hydrogen atoms is dictated by the proton–proton avoidance rule, so that the neighbouring atoms never occupy equivalent crystallographic sites. The long-range distribution of proton pairs is uncorrelated, and, in general, instantaneous configuration of protons violates all symmetry elements of SG *Pbnm*.

In contrast, X-ray and neutron diffraction techniques give averaged atomic arrangements over many unit cells and a dynamic average over a time interval for each measurement which is in the order of seconds. According to the results of our simulations, many random transitions of protons between allowed crystallographic sites in different unit cells take place during the XRD measurement. Therefore, proton dynamics in topaz-OH are averaged in the XRD and neutron diffraction pattern. The time-averaged symmetric distribution of protons at room and high temperatures is obvious from Fig. 5b. Mirror planes are easily recognized. Thus, both XRD and neutron diffraction pattern of topaz-OH can be refined in SG *Pbnm*.

Qualitative differences in the proton distribution at room temperature and at 55 K (Fig. 5b) raise the question of a possible order–disorder phase transition in topaz-OH at very low temperature. Since thermal hopping of protons takes place even at room temperature, the classical free energy barrier for transitions is small. Therefore, in approximation of the classical nuclei, an order–disorder phase transition would occur at rather low temperature. However, quantum motion of protons would smear out the classical free energy barrier and the order–disorder phase transition might therefore not be observed at low temperature. Thus, to prove the existence of a low-temperature order–disorder phase transition in topaz-OH, a direct quantitative estimation of the free energy barrier for proton transition in approximation of classical nuclei and quantum simulations is necessary.

Acknowledgements The authors are grateful to Dr. M. Iannuzzi, Prof. M. Bernasconi and Prof. M. Parrinello for fruitful discussions. We appreciate access to computational facilities of the Potsdam Institute for Climate Impact Research and CSCS-Manno. The authors also thank two anonymous readers for their thoughtful reviews.

References

Barton MD (1982) The thermodynamic properties of topaz solid solution and some petrological applications. Am Mineral 67: 956–974

Becke AD (1988) Density-functional exchange-energy approximation with correct asymptotic behaviour. Phys Rev (A) 38(6): 3098–3100

Blöchl PE, Parrinello M (1992) Adiabaticity in first-principles molecular dynamics. Phys Rev (B) 5(16): 9413–9416

Borysow J, Moraldi M, Frommhold L (1985) The collision-induced spectroscopies concerning the desymetrisation of classical lineshape. Mol Phys 56(4): 913–922

Car R, Parrinello M (1985) Unified approach for molecular dynamics and density-functional theory. Phys Rev Lett 55(22): 2471–2474

CPMD, Copyright IBM corp. (1990–2001) Copyright MPI für Festkörperforschung, Stuttgart, 1997–2001

Domanik KJ, Holloway JR (1996) The stability and composition of phengitic muscovite and associated phases from 5.5 to 11 GPa: implications for deeply subducted sediments. Geochim Cosmochim Acta 60(21): 4133–4150

Egelstaff PA (1962) Neutron scattering studies of liquid diffusion. Adv Phys 11(43): 203–232

Ferrando S, Frezzotti L, Alberico A, Compagnoni R (2002) Petrologic and fluid inclusion study of an OH-rich topaz-bearing kyanite quarzite from Sulu UHP terrane, Eastern China. J Conf EMPG. IX Zurich, Swiss; 24–27 March 2002 Abs 7: 32

Gebert W, Zemann J (1965) Messung des Ultrarot-Pleochroismus von Mineralen. III. Der Pleochroismus der OH-Streckfrequenz in Topas. N Jb Min Mh: 380–384

Goedecker S, Teter M, Hutter J (1996) Separable dual-space Gaussian pseudopotentials. Phys Rev (B) 54(3): 1703–1710

Iannuzzi M, Parrinello M (2001) Efficient k·p method for the calculation of total energy and electronic density of states. Phys Rev (B) 64(23): 233104–233108

Karki BB, Stixrude L, Clark SJ, Warren MC, Ackland GJ, Crain J (1997) Elastic properties of orthorombic $MgSiO_3$ perovskite at lover mantle pressures. Am Mineral 82: 635–638

Lee CL, Yang W, Parr RG (1988) Development of the Colle–Salventti correlation energy formula into a functional of the electron density. Phys Rev (B) 37(2): 785–789

Monkhorst HJ, Pack D (1975) Special points for Brellouin-zone integration. Phys Rev (B) 13: 5188–5192

Northrup PA, Leinenweber K, Parise JB (1994) The location of H in the high-pressure synthetic $Al_2SiO_4(OH)_2$ topaz analogue. Am Mineral 79: 401–404

Press WH, Teukolsky SA, Vetterling WT, Flannery BP (1992) Numerical recipes. The art of scientific computing. Cambridge University Press, Cambridge

Schmidt MW (1995) Lawsonite: upper pressure stability and formation of higher density hydrous phases. Am Mineral 80: 1286–1292

Schreyer W (1995) Ultradeep metamorphic rocks: the retrospective viewpoint. J Geophys Res 100(B5): 8353–8366

Silvestrelli PL, Bernasconi M, Parrinello M (1997) Ab initio infrared spectrum of liquid water. Chem Phys Lett 277: 478–482

Sprik M, Hutter J, Parrinello M (1996) Ab initio molecular dynamics simulation of liquid water: comparison of three gradient-corrected density functionals. J Chem Phys 105(3): 1142–1152

Terhune RW, Peters CW (1959) Electric field-induced vibration rotation spectrum of H2 and D2. J Mol Spect 3(2): 138–147

Troullier N, Martins JL (1991) Efficient pseudopotentials for plane-wave calculations. Phys Rev (B) 43: 1993–2006

Wunder B, Rubie DC, Ross II CR, Medenbach O, Seifert F, Schreyer W (1993) Synthesis, stability, and properties of $Al_2SiO_4(OH)_2$: a fully hydrated analogue of topaz. Am Mineral 78: 285–297

Wunder B, Andrut M, Wirth R (1999) High-pressure synthesis and properties of OH-rich topaz. Eur J Miner 11: 803–813

Zhang RY, Liou JG, Shu JF (2002) Hydroxyl-rich topaz in high-pressure and ultrahigh-pressure kyanite quartzites, with retrograde woodhousite, from the Sulu terrane, eastern China. Am Mineral 87: 445–453